Letter

Three-body unitary coupled-channel analysis on $\eta(1405/1475)$

S. X. Nakamura,[1,2,*] Q. Huang,[3] J.-J. Wu,[4,†] H. P. Peng,[1,2] Y. Zhang,[1,2] and Y. C. Zhu[1,2]

[1]*University of Science and Technology of China, Hefei 230026, China*
[2]*State Key Laboratory of Particle Detection and Electronics (IHEP-USTC), Hefei 230036, China*
[3]*Department of Physics, Nanjing Normal University, Nanjing, Jiangsu 210097, China*
[4]*School of Physical Sciences, University of Chinese Academy of Sciences (UCAS), Beijing 100049, China*

(Received 23 December 2022; accepted 4 May 2023; published 25 May 2023)

The recent BESIII data on $J/\psi \to \gamma(K_S K_S \pi^0)$, which is significantly more precise than earlier $\eta(1405/1475)$-related data, enables quantitative discussions on $\eta(1405/1475)$ at the previously unreachable level. We conduct a three-body unitary coupled-channel analysis of experimental Monte Carlo outputs for radiative J/ψ decays via $\eta(1405/1475)$: $K_S K_S \pi^0$ Dalitz plot distributions from the BESIII, and branching ratios of $\gamma(\eta\pi^+\pi^-)$ and $\gamma(\gamma\pi^+\pi^-)$ final states relative to that of $\gamma(K\bar{K}\pi)$. Our model systematically considers (multi)loop diagrams and an associated triangle singularity, which is critical for making excellent predictions on $\eta(1405/1475) \to \pi\pi\pi$ line shapes and branching ratios. The $\eta(1405/1475)$ pole locations are revealed for the first time. Two poles for $\eta(1405)$ are found on different Riemann sheets of the $K^*\bar{K}$ channel, while one pole is found for $\eta(1475)$. The $\eta(1405/1475)$ states are described by two bare states dressed with continuum states. The lower bare state would be an excited η', while the higher one could be an excited $\eta^{(\prime)}$, hybrid, glueball, or a mixture of these. This work presents the first-ever pole determination based on a manifestly three-body unitary coupled-channel framework applied to experimental three-body final state distributions (Dalitz plots).

DOI: 10.1103/PhysRevD.107.L091505

I. INTRODUCTION

The nature of isoscalar pseudoscalar meson(s) in the 1.4–1.5 GeV region, $\eta(1405/1475)$, has been controversial. On the experimental side, two different states seem to work for $K\bar{K}\pi$ final states produced in $\pi^- p$ scattering [1,2], $p\bar{p}$ annihilations [3], and radiative J/ψ decays [4,5]. However, only one resonant peak, whose position is somewhat process dependent, is observed in the following: $\eta\pi\pi$ final states in $p\bar{p}$ annihilation [6] and J/ψ decays accompanied by γ [7–9] and ω [10]; $K\bar{K}\pi$ and $\eta\pi\pi$ final states in $\gamma\gamma$ collisions [11]; and $\gamma\rho^0$ final states in radiative J/ψ decays [9,12,13] and $p\bar{p}$ annihilation [6]. These data are statistically limited, allowing various theoretical descriptions. In particular, whether $\eta(1405/1475)$ is one or two states remains as a major puzzle.

The quark model predicts only one state, a radially excited $\eta'(958)$, in this energy region, and the ideal mixing $(s\bar{s})$ [14,15] seems consistent with a lattice QCD (LQCD) [16]. To accommodate two states, $\eta(1405)$ was proposed as a glueball [17]; however, it is disfavored by LQCD predicting a significantly heavier mass [18–22]. The $\eta(1405/1475)$ couples to quasi-two-body channels such as $K^*\bar{K}$ and $a_0\pi$, which further decay to three-body channels such as $K\bar{K}\pi$ and $\pi\pi\eta$, forming a complicated coupled-channel system. In addition, a kinematical triangle singularity is caused by the coupled-channel dynamics and plays an important role [23–26]. Thus, a sophisticated coupled-channel analysis of high quality data has been long-awaited to determine the nature of $\eta(1405/1475)$.

The recent high-statistics BESIII experiment provides a good opportunity to improve our understanding of $\eta(1405/1475)$. They collected $\sim 10^{10} J/\psi$ decay samples and conducted an amplitude analysis on $J/\psi \to \gamma(K_S K_S \pi^0)$ [27]. Their bin-by-bin analysis of the $K_S K_S \pi^0$ invariant mass extracted a $J^{PC} = 0^{-+}$ contribution. Then, their energy-dependent analysis identified two $\eta(1405/1475)$ states with a high statistical significance and determined their Breit-Wigner (BW) masses and widths. However, the BW amplitude does not respect the unitary and is therefore not suitable in situations where more than one resonance are overlapping and/or a resonance is close to its decay channel threshold [28]; the situations apply to $\eta(1405)$ and $\eta(1475)$ that are overlapping, and $\eta(1405)$ being close to the $K^*\bar{K}$ threshold. Thus, an important issue is to determine

*satoshi@ustc.edu.cn
†wujiajun@ucas.ac.cn

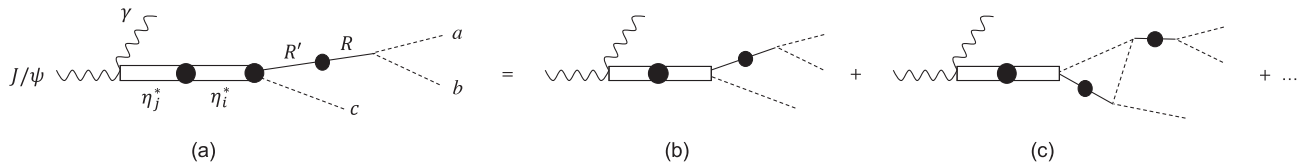

FIG. 1. (a) Radiative J/ψ decay model. The dashed and solid lines represent pseudoscalar mesons and bare two-meson resonances R, respectively. The double lines represent bare $\eta(1405/1475)$ states. Dressed propagators and vertices are represented by the solid circles. The main η^* decay mechanisms are (b) direct decays and (c) single triangle mechanisms.

the $\eta(1405/1475)$ pole locations, which can be achieved by analytically continuing a unitary coupled-channel J/ψ decay amplitude fitted to the BESIII data.

Another puzzling issue is a large isospin violation in $\eta(1405/1475) \to \pi\pi\pi$ [29]. An explanation has been proposed in Refs. [23–25]: the $K^*\bar{K}K$-loop mechanism involving a triangle singularity significantly amplifies the isospin violation due to the mass difference between $K^\pm$ and K^0. Now, the issue is to confirm this explanation by examining whether the three-body unitary coupled-channel model fitted to the recent BESIII data [27] can also consistently describe line shapes and branchings of the three-pion final states; the triangle singularity mechanism is automatically included in the unitary framework.

In this work,[1] we conduct a coupled-channel analysis of radiative J/ψ decays via $\eta(1405/1475)$. Our three-body unitary coupled-channel model is fitted to $K_SK_S\pi^0$ Dalitz plot distributions from the BESIII Monte Carlo (MC) simulation [27], as well as to branching fractions of $\eta\pi^+\pi^-$ and $\rho^0\gamma$ relative to that of $K\bar{K}\pi$. The model will clarify the main $\eta(1405/1475)$ decay mechanisms and predict $\eta(1405/1475) \to \eta\pi\pi, \pi\pi\pi$ line shapes and branchings. The analysis addresses three major puzzles regarding $\eta(1405/1475)$:

(i) Process-dependent line shapes of $\eta(1405/1475)$ decays.
(ii) Large isospin violation in $\eta(1405/1475) \to \pi\pi\pi$.
(iii) One or two states of $\eta(1405/1475)$, equivalently, pole structure.

II. MODEL

Our three-body unitary coupled-channel model is primarily based on the formulation in Refs. [31,32]. Similar three-body unitary formulations were presented recently [33–35]. A notable extension here is to consider charge-dependent particle masses for describing the isospin violations. Thus, a radiative J/ψ decay amplitude[2] via $\eta(1405/1475)$ excitations is diagrammatically represented in Fig. 1(a) and given by

$$A_{\gamma abc,J/\psi} = \sum_{abc}^{\text{cyclic}} \sum_{RR's_R^z} \sum_{ij} \Gamma_{ab,R}\tau_{R,R'}(p_c, E - E_c) \times \bar{\Gamma}_{cR',\eta_i^*}(\boldsymbol{p}_c, E)\bar{G}_{ij}(E)\Gamma_{\gamma\eta_j^*,J/\psi}, \quad (1)$$

where a, b, and c are pseudoscalar mesons (π, K, η), and R denotes a two-meson resonance such as K^*, $K_0^*(700)(=\kappa)$, $a_0(980)$, and $f_0(980)$; cyclic permutations $(abc), (cab), (bca)$ are indicated by $\sum_{abc}^{\text{cyclic}}$; the indices i and j specify one of the bare η^* states; and E denotes the abc total energy in the abc center-of-mass (CM) frame. We introduce a $J/\psi \to \gamma\eta_i^*$ vertex ($\Gamma_{\gamma\eta_j^*,J/\psi}$), a dressed η^* propagator ($\bar{G}_{ij}$), a dressed $\eta_i^* \to Rc$ vertex ($\bar{\Gamma}_{cR,\eta_i^*}$), a dressed R propagator ($\tau_{R,R'}$), and an $R \to ab$ vertex ($\Gamma_{ab,R}$).

The dressed R propagator matrix is

$$[\tau^{-1}(p,E)]_{R,R'} = [E - E_R(p)]\delta_{R,R'} - [\Sigma(p,E)]_{R,R'}, \quad (2)$$

where a matrix $\Sigma_{R,R'}$ is the R self-energy caused by $\Gamma_{ab,R}$. The dressed $\eta_i^* \to Rc$ vertices are

$$\bar{\Gamma}_{cR,\eta_i^*}(\boldsymbol{p}_c, E) = \int d^3q\, \Phi_{cR,c'R'}(\boldsymbol{p}_c, \boldsymbol{q}; E)\Gamma_{c'R',\eta_i^*}(\boldsymbol{q}), \quad (3)$$

with $\sum_{c'R's_{R'}^z}$ being implicit; $\Phi = (1 - \int d^3qV\tau)^{-1}$ is a wave function, and Γ_{cR,η_i^*} is a bare $\eta_i^* \to Rc$ vertex. The $Rc \to R'c'$ interaction V includes Z diagrams in which $R \to c'\bar{c}$ is followed by $\bar{c}c \to R'$ via a $\bar{c}$ exchange. An isospin-violating $K^*\bar{K} \to f_0\pi$ process is caused by a K-exchange Z diagram and $m_{K^\pm} \neq m_{K^0}$. Formulas for the Z diagrams can be found in Appendix C of Ref. [31]. In addition, V includes vector-meson exchange mechanisms, based on the hidden local symmetry model [36], for $K^*\bar{K} \leftrightarrow K^*\bar{K}, \bar{K}^*K$; see Appendix A of Ref. [32] for formulas. The nonperturbative treatment of $V\tau$ in Eq. (3) is a requirement from the three-body unitarity.

The dressed η^* propagator is

$$[\bar{G}^{-1}(E)]_{ij} = (E - m_{\eta_i^*})\delta_{ij} - [\Sigma_{\eta^*}(E)]_{ij}, \quad (4)$$

where $m_{\eta_i^*}$ is the bare mass and the η^* self-energy is

$$[\Sigma_{\eta^*}(E)]_{ij} = \sum_{cRR's_R^z} \int d^3q\, \Gamma_{cR,\eta_i^*}(\boldsymbol{q}) \times \tau_{R,R'}(q, E - E_c(q))\bar{\Gamma}_{cR',\eta_j^*}(\boldsymbol{q}, E). \quad (5)$$

[1] A fuller account of this work will be given separately [30].
[2] We denote a particle x's mass, momentum, energy, spin, and z component in the abc center-of-mass frame by $m_x, \boldsymbol{p}_x, E_x, s_x$, and s_x^z, respectively; $E_x = \sqrt{m_x^2 + |\boldsymbol{p}_x|^2}$. The mass values are from Ref. [14].

The coupled channels included in our default model are two bare η^* states and $Rc = K^*(892)\bar{K}$, $\kappa\bar{K}$, $a_0(980)\pi$, $a_2(1320)\pi$, $f_0\eta$, $\rho(770)\rho(770)$,[3] and $f_0\pi$: $\bar{K}^*(892)K$ and $\bar{\kappa}K$ are implicitly included to form positive C-parity states. The bare R states and their decay channels (two-meson continuum states) couple nonperturbatively to generate scattering amplitudes and resonance poles. Thus, we can fix the coupling and cutoff parameters in $\Gamma_{ab,R}$ and m_R (bare mass) by fitting $ab \to ab$ scattering data. Meanwhile, real and complex coupling parameters in Γ_{cR,η_i^*} and $\Gamma_{\gamma\eta_i^*,J/\psi}$, respectively, and $m_{\eta_i^*}$ are fitted to MC outputs for $J/\psi \to \gamma\eta(1405/1475) \to \gamma(abc)$ as detailed in Sec. III A; cutoffs of dipole form factors in Γ_{cR,η_i^*} are fixed to 700 MeV. To describe the $\gamma(\pi^+\pi^-\gamma)$ final state, we assume the vector-meson dominance mechanism where $\rho\rho$ from the dressed $\eta_i^* \to \rho\rho$ is followed by $\rho \to \gamma$ and $\rho \to \pi^+\pi^-$, with no additional parameters. We have 25 fitting parameters in total.

III. RESULTS

A. Fit and comparison with data

Using the $J^{PC} = 0^{-+}$ partial wave amplitude from the BESIII MC (E-dependent solution) for $J/\psi \to \gamma K_S K_S \pi^0$ [27], we generate $K_S K_S \pi^0$ Dalitz plot pseudodata for each of 30 E bins (10-MeV bin width; labeled by l) in the range of $1300 \le E \le 1600$ MeV. The pseudodata are thus detection efficiency corrected and background-free. The Dalitz plot for an lth E bin is further binned by equally dividing $(0.95\ \text{GeV})^2 \le m^2_{K_S K_S} \le (1.50\ \text{GeV})^2$ and $(0.60\ \text{GeV})^2 \le m^2_{K_S\pi^0} \le (1.15\ \text{GeV})^2$ into 50×50 bins (labeled by m); m_{ab} is the ab invariant mass. The pseudodata include $\sim 1.23 \times 10^5$ events in total, consistent with the BESIII data. The event numbers in the $\{l, m\}$ and lth bins are $N_{l,m}$ and $\bar{N}_l (\equiv \sum_m N_{l,m})$, respectively, with statistical uncertainties $\sqrt{N_{l,m}}$ and $\sqrt{\bar{N}_l}$, respectively. Fitting $\{N_{l,m}\}$ and $\{\bar{N}_l\}$ pseudodata would constrain the detailed decay dynamics and the resonant behavior (pole structure) of $\eta(1405/1475)$, respectively. We generate and fit 50 pseudodata samples to estimate the statistical uncertainty of the model with the bootstrap method [37].

Ratios of partial decay widths are also fitted: $R_1^{\text{exp}} = \Gamma[J/\psi \to \gamma\eta(1405/1475) \to \gamma(K\bar{K}\pi)]/\Gamma[J/\psi \to \gamma\eta(1405/1475) \to \gamma(\eta\pi^+\pi^-)] \sim 6.8$–$11.9$ [14] and $R_2^{\text{exp}} = \Gamma[J/\psi \to \gamma\eta(1405/1475) \to \gamma(\rho^0\gamma)] / \Gamma[J/\psi \to \gamma\eta(1405/1475) \to \gamma(K\bar{K}\pi)] = 0.015$–$0.043$ [12,13]. We calculate the partial widths Γ by integrating the E distributions for the $K\bar{K}\pi$, $\pi^+\pi^-\eta$, and $\pi^+\pi^-\gamma$ final states over the range of $1350\ \text{MeV} < E < 1550\ \text{MeV}$. The above ratios can constrain parameters associated with the $f_0\eta$ and $\rho\rho$ channels that are not well determined by the $K_S K_S \pi^0$ Dalitz plots.

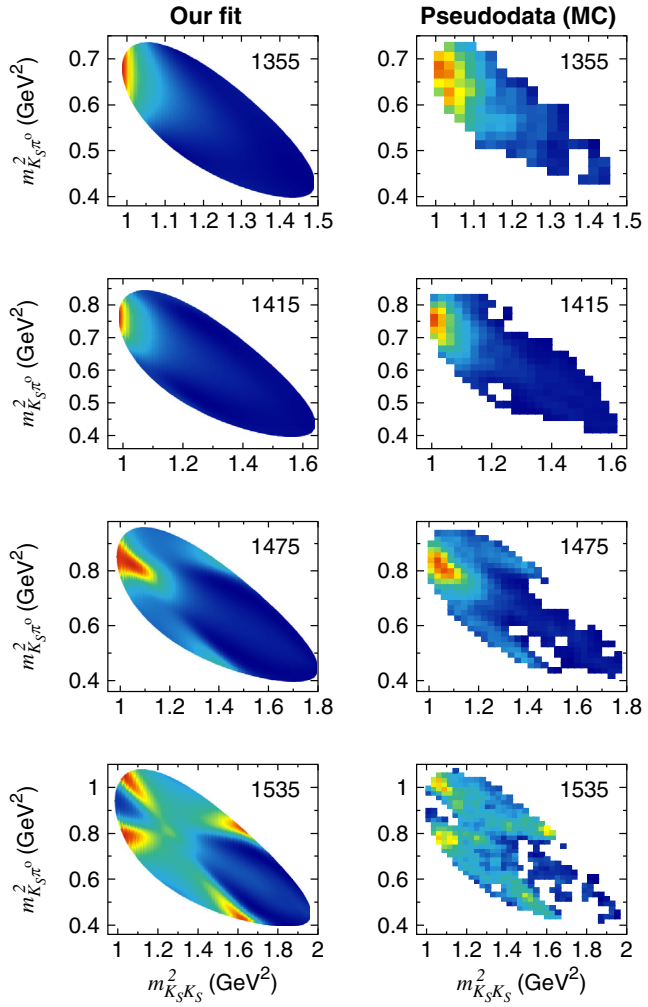

FIG. 2. Dalitz plot distributions of $J/\psi \to \gamma\eta(1405/1475) \to \gamma(K_S K_S \pi^0)$. The E values (MeV) used in our calculation (central values of the MC E bins) are indicated.

Our default model is simultaneously fitted to the MC-based $\{N_{l,m}\}$, $\{\bar{N}_l\}$, R_1^{exp}, and R_2^{exp} with a χ^2-minimization, with no direct fit to the actual BESIII data. To keep a reasonable computational cost for calculating χ^2 from $\{N_{l,m}\}$, we compare $N_{l,m}$ with the differential decay width evaluated at the bin center and multiplied by the bin volume. Accordingly, $N_{l,m}$ on the phase-space boundary are omitted from the χ^2 calculation. In addition, a bin of $N_{l,m} < 10$ is combined with neighboring bins so that bins with more than nine events are included in the χ^2 calculation. The number of bins for $\{N_{l,m}\}$ is 4496–4575, depending on the pseudodata samples. Note that χ^2 from $\{\bar{N}_l\}$, R_1^{exp}, and R_2^{exp} are appropriately weighted so that these data can reasonably constrain the model. By fitting the 50 samples, we obtain $\chi^2/\text{ndf} = 1.40$–1.54

[3]The $\rho\rho$ channel needs slight modifications of the presented formulas; see Ref. [30].

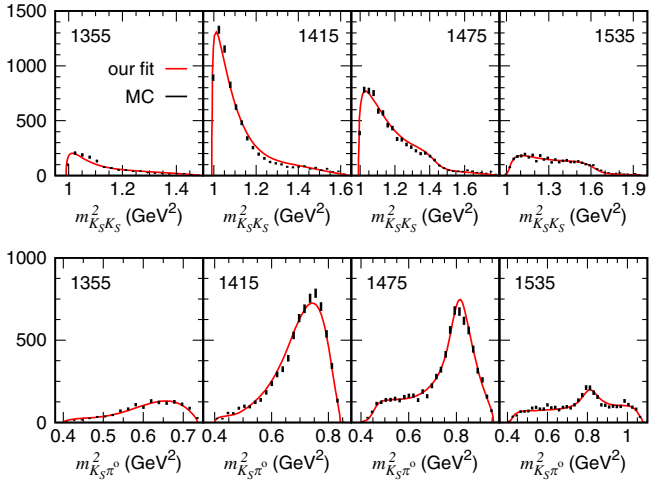

FIG. 3. The K_SK_S (upper panels) and $K_S\pi^0$ (lower) invariant mass distributions (events/bin). The E values (MeV) are indicated.

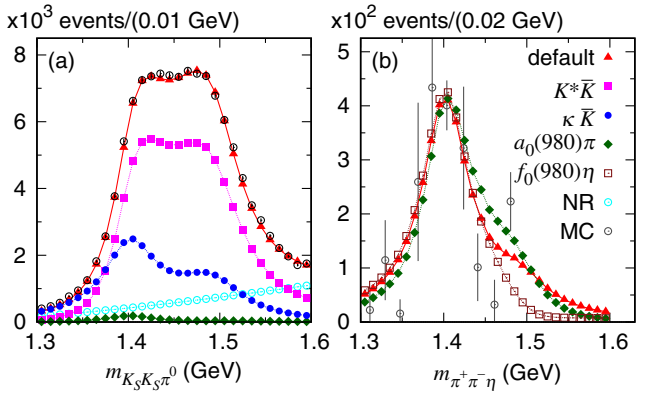

FIG. 4. The E distributions for $J/\psi \to \gamma\eta(1405/1475) \to$ (a) $\gamma(K_SK_S\pi^0)$ and (b) $\gamma(\pi^+\pi^-\eta)$. The default, final Rc, and nonresonant (NR) contributions, and MC outputs [Ref. [27] in (a), Ref. [7] in (b)] are shown. Lines connecting the points are guides to the eye.

(ndf: number of degrees of freedom) from comparing with $\{N_{l,m}\}$, and $R_1^{\rm th} \sim 7.5$ and $R_2^{\rm th} \sim 0.025$.

In Fig. 2, we show the $K_SK_S\pi^0$ Dalitz plot distributions, at representative E values, from one of the pseudodata samples and our default fit to them.[4] Their patterns agree well overall. The $a_0(980)$-like peak is clearly seen near the K_SK_S threshold for $1.3 \lesssim E \lesssim 1.44$ GeV, while the K^* peak is clear for $1.5 \lesssim E \lesssim 1.6$ GeV. Good-quality fits are more clearly shown in Fig. 3 where the $a_0(980)$-like and $K^*(892)$ peak structures in the K_SK_S and $K_S\pi^0$ invariant mass distributions, respectively, are well reproduced. The absolute values of the distributions are large in the $\eta(1405/1475)$ peak region ($E = 1.4$–1.5 GeV). By integrating the distributions at each E, we obtain the E distribution shown in Fig. 4(a).

We show contributions from the main $\eta^* \to K\bar{K}\pi$ decay mechanisms. The η^* decay mechanisms can be classified according to *final Rc* states in Fig. 1(a) that directly couple to the final *abc* states. As shown in Fig. 4(a), the final $K^*\bar{K}$ and $\kappa\bar{K}$ give the first and second largest contributions, respectively. The clear $a_0(980)$-like peak in the K_SK_S invariant mass spectra (Fig. 3) is mostly formed by a constructive interference within the final Bose-symmetrized $K_S^*K_S \to \pi^0K_SK_S$ contribution at the K_SK_S threshold; the small final $a_0(980)\pi$ contribution slightly sharpens the peak through an interference.

Our decay mechanisms are rather different from the BESIII MC [27], where the $a_0(980)\pi$ contribution is the largest overall, and the $K^*\bar{K}$ contribution is comparable only at $E \sim 1500$ MeV. There are three important improvements in our model: including the $\kappa\bar{K}$ channel, fitting the ratio $R_1^{\rm exp}$, and accounting for the coupled-channel effects. The large $R_1^{\rm exp}$ is, albeit a large uncertainty, an important constraint on the final $a_0(980)\pi$ contribution to $K\bar{K}\pi$ since the coupling magnitude of $a_0(980) \to K\bar{K}$ relative to $a_0(980) \to \pi\eta$ is determined experimentally [38]. Our $a_0(980)\pi$ contribution to fit $R_1^{\rm exp}$ is small, and the final $\kappa\bar{K}$ contribution is significant.

Among the coupled-channel mechanisms included in Fig. 1(a), direct decays [Fig. 1(b)] and single triangle mechanisms [Fig. 1(c)] play an important role. The direct-decay and single-triangle mechanisms are dominant in the final $K^*\bar{K}$ and $\kappa\bar{K}$ contributions, respectively, while they are comparable in the final $a_0(980)\pi$ contribution. Figure 4(a) shows that the broad peak structure from the full calculation is mainly formed by the final $K^*\bar{K}$ contribution.

To address whether $\eta(1405/1475)$ is one or two states, we attempt to fit the BESIII MC output for $K_SK_S\pi^0$ with a single bare η^* model. The final $\kappa\bar{K}$ and $a_0\pi$ contributions have similar line shapes peaking at $E \sim 1420$ MeV, while the final $K^*\bar{K}$ contribution has a peak 30–40 MeV higher since $K^*\bar{K}$ is relatively a p-wave and its threshold is at $E \sim 1400$ MeV. Their coherent sum cannot reproduce the ~100-MeV wide flat peak, even if only fitting the E distribution. We thus conclude that two bare η^* states are necessary to explain the 0^{-+} contribution of the BESIII MC.

Now, our default model makes predictions for $\eta^* \to \pi\pi\pi$ and $\pi\pi\eta$. The predicted E dependence for $J/\psi \to \gamma\eta(1405/1475) \to \gamma(\eta\pi^+\pi^-)$ is shown in Fig. 4(b). The line shape is consistent with the MC [7,8]. Although both $K\bar{K}\pi$ and $\pi\pi\eta$ originate from the same resonance(s), the $\pi\pi\eta$ final states give a single peak at $m_{\pi\pi\eta} \sim 1400$ MeV while the $m_{K\bar{K}\pi}$ distribution has a broad peak. This is because $K\bar{K}\pi$ and $\pi\pi\eta$ are from different final Rc states that have different E dependence. As shown in Fig. 4(b), the comparable final $a_0(980)\pi$ and $f_0\eta$ contributions explain

[4]Figures 2 (right), 3, and 4(a) show the same pseudodata.

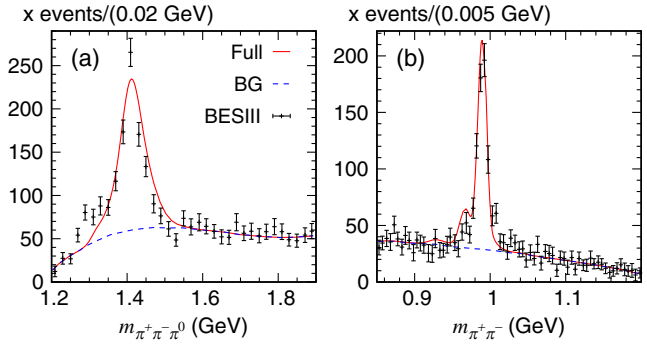

FIG. 5. (a) The $m_{\pi^+\pi^-\pi^0}$ and (b) $m_{\pi^+\pi^-}$ distributions for $J/\psi \to \gamma(\pi^+\pi^-\pi^0)$. Our full results have been smeared with the bin width, scaled to fit the BESIII data [29], and augmented by the background polynomials (BG) of [29].

the full result for the $\pi\pi\eta$ final states. On the other hand, the $K\bar{K}\pi$ final states are mainly from the final $K^*\bar{K}$ and $\kappa\bar{K}$ contributions, as seen in Fig. 4(a). This explains the process dependence of the $\eta(1405/1475)$ line shapes.

For the isospin-violating $J/\psi \to \gamma\eta(1405/1475) \to \gamma(\pi\pi\pi)$, our coupled-channel model predicts the $m_{\pi^+\pi^-\pi^0}$ and $m_{\pi^+\pi^-}$ distributions as shown in Figs. 5(a) and 5(b), respectively, in good agreement with the BESIII data [29]. The authors of Refs. [23,24,26] proposed that these processes are dominantly caused by the $K^*K\bar{K}$ triangle loop mechanisms [Fig. 1(c)]. While the $K^*K^+K^-$ and $K^*K^0\bar{K}^0$ triangle loops cancel each other almost exactly for the isospin symmetry, due to $m_{K^\pm} \neq m_{K^0}$, a significant isospin violation occurs in the small window of $2m_{K^\pm} \lesssim m_{\pi^+\pi^-} \lesssim 2m_{K^0}$. The mechanism satisfies the kinematical condition to cause a triangle singularity at $m_{\pi^+\pi^-\pi^0} \sim 1410$ MeV and $m_{\pi^+\pi^-} \sim 2m_K$, and the peaks appear as a result, as shown in Fig. 5. This mechanism is required by the three-body unitarity; thus, it is automatically included in our calculation.

The $K\bar{K}\pi$ and $\pi\pi\pi$ branching ratios in Refs. [14,29] give the following ratios: $\Gamma[J/\psi \to \gamma\eta(1405/1475) \to \gamma(\pi^+\pi^-\pi^0)]/\Gamma[J/\psi \to \gamma\eta(1405/1475) \to \gamma(K\bar{K}\pi)] = 0.004$–$0.007$ and $\Gamma[J/\psi \to \gamma\eta(1405/1475) \to \gamma(\pi^0\pi^0\pi^0)]/\Gamma[J/\psi \to \gamma\eta(1405/1475) \to \gamma(K\bar{K}\pi)] = 0.002$–$0.003$. Our coupled-channel model predicts 0.0045–0.0047 and 0.0015–0.0016, respectively, in good agreement with the experimental ones. These reasonable predictions for the $\pi\pi\eta$ and $\pi\pi\pi$ final states support the model's dynamical content.

B. Pole structure of $\eta(1405/1475)$

Extraction of poles from amplitudes that respect three-body unitarity has long been discussed [39–41]. However, until recently, this method had not been applied to data involving three-body final states. A breakthrough was made by extracting an $a_1(1260)$ pole from $m_{\pi^+\pi^-\pi^-}$ lineshape data for $\tau^- \to \pi^+\pi^-\pi^-\nu_\tau$ with a $\rho\pi$ single-channel model [42,43]. The three-body unitarity was rigorously (partially) considered in Ref. [43] ([42]). Consequently, an additional spurious pole was found in Ref. [42], indicating the importance of the full three-body unitarity for studying pole structures. The analysis method of Ref. [43] should be further improved by considering coupled channels and fitting Dalitz plots. Below, we extract $\eta(1405/1475)$ poles with such improvements; the three-body unitarity is treated as rigorously as in Ref. [43].

TABLE I. Pole positions (E_{η^*}) labeled by α. The mass and width are $M = \mathrm{Re}[E_{\eta^*}]$ and $\Gamma = -2\mathrm{Im}[E_{\eta^*}]$, respectively. The Riemann sheet (RS) of E_{η^*} is specified by $(s_{K^*\bar{K}}, s_{a_2(1320)\pi})$ where $s_x = p(u)$ indicates the physical (unphysical) sheet of a channel x. The BESIII result shows Breit-Wigner parameters. All errors are statistical.

	M (MeV)	Γ (MeV)	RS
$\alpha = 1$	1401.6 ± 0.6	65.8 ± 1.0	(up)
$\alpha = 2$	1401.6 ± 0.6	66.3 ± 0.9	(pp)
$\alpha = 3$	1495.0 ± 1.5	86.4 ± 1.8	(up)
BESIII [27]	1391.7 ± 0.7	60.8 ± 1.2	
	1507.6 ± 1.6	115.8 ± 2.4	

We search for $\eta(1405/1475)$ poles (E_{η^*}) that satisfy $\det[\bar{G}^{-1}(E_{\eta^*})] = 0$ with $\bar{G}^{-1}(E)$ defined in Eq. (4). The analytic continuation of $\bar{G}^{-1}(E)$ involves appropriately deforming the integral paths in Eqs. (3) and (5) to avoid crossing singularities and to select a relevant Riemann sheet (RS) [39–41,43,44]. Our analytic continuation method is quite similar to that described in Ref. [43].

Three poles labeled by $\alpha = 1, 2$ [$\alpha = 3$] corresponding to $\eta(1405)$ [$\eta(1475)$] are found; see Table I. Statistical errors are based on 50 bootstrap fits. Although the mass and width values from our analysis and the BESIII analysis (BW parameters) do not agree within the errors, they are fairly similar. The poles are close to the branch points associated with the $K^*(892)\bar{K}$ and $a_2(1320)\pi$ channels, as shown in Fig. 6. Thus, we specify the RS of these channels in Table I.[5] The two-pole structure of $\eta(1405)$ does not mean two physical states but is simply due to the fact that a pole is split into two poles on different RSs of its decay channel. The two $\eta(1405)$ pole values are very similar except for the RS due to their proximity to the $K^*(892)\bar{K}$ threshold. As a consequence of the unitarity, the pole structure (η^* propagation) and the Dalitz plot distributions (η^* decay mechanism) are connected by the common dynamics in our model but not in the BW model.

The bare states in our model are conceptually similar to states given by quark models or LQCD without two-hadron operators. The new BESIII data [27] require two bare states. The lighter one, ~1.6 GeV, seems compatible with the excited $s\bar{s}$ [14,15]. The heavier bare mass can be in the range of 2–2.4 GeV to give comparable fits. This state

[5]Section 50 of Ref. [14] defines the (un)physical sheet.

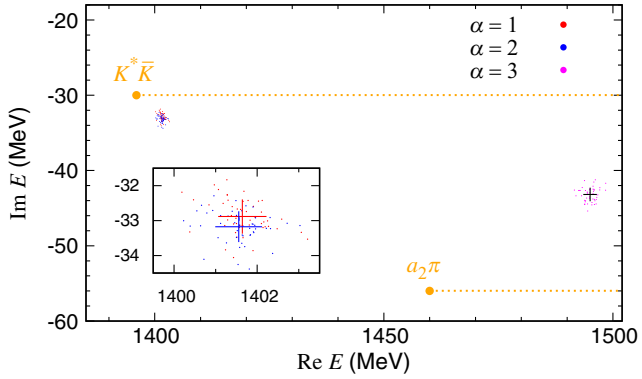

FIG. 6. Pole locations labeled by α from 50 bootstrap fits. The crosses indicate averaged pole locations and their standard deviations. The orange circles and dotted lines are the $K^*(892)\bar{K}$ and $a_2(1320)\pi$ branch points and cuts, respectively. The $\alpha = 1, 2$ region is enlarged in the inset.

could be either of a second radial excitation of $\eta^{(\prime)}$, a hybrid [16], a glueball [18–22], or their mixture. The two bare states are mixed and dressed by continuum coupled channels to form the $\eta(1405/1475)$ poles.

IV. SUMMARY AND OUTLOOK

We conducted a coupled-channel analysis of radiative J/ψ decays via $\eta(1405/1475)$ and addressed the long-standing $\eta(1405/1475)$ puzzles itemized in the Introduction. Our three-body unitary coupled-channel model is reasonably fitted to the $K_S K_S \pi^0$ Dalitz plot pseudodata samples generated with $J^{PC} = 0^{-+}$ amplitude of the BESIII MC [27], and also to branching fractions of $\eta\pi^+\pi^-$ and $\gamma\pi^+\pi^-$ final states relative to that of $K\bar{K}\pi$. The model predicts the different $\eta(1405/1475)$ line shapes for the $\eta\pi^+\pi^-$ and $\pi\pi\pi$ final states in reasonable agreement with experimental results. The model also predicts the branching fractions well for the isospin-violating $\pi\pi\pi$ final states and their narrow $f_0(980)$-like $\pi^+\pi^-$ line shape; the triangle singularity effect automatically included in our unitary model plays a crucial role. Our model revealed the $\eta(1405/1475)$ pole structure for the first time. Two poles on different Riemann sheets of the $K^*\bar{K}$ channel correspond to $\eta(1405)$, and one pole corresponds to $\eta(1475)$.

Finally, we presented the first pole determination based on a manifestly three-body unitary coupled-channel framework applied to experimental Dalitz plot distributions. In the future, the present analysis for 0^{-+} should be further extended to include more J^{PC} to analyze the radiative J/ψ decay data directly, consistently addressing pole structures of $\eta(1405/1475)$, $f_1(1420)$, etc. with the unitary coupled-channel framework. This development is important since the present analysis results could have been biased by the 0^{-+} components in the radiative J/ψ decays determined with simpler Breit-Wigner models [7,8,12,13,27].

ACKNOWLEDGMENTS

The authors thank the BESIII Collaboration for providing us with the MC outputs for our study. The authors also thank Jozef J. Dudek, T.-S. Harry Lee, Bei-Jiang Liu, Xiao-Hai Liu, Toru Sato, Guo-Fa Xu, Qiang Zhao, and Bing-Song Zou for useful discussions. This work is, in part, supported by the National Natural Science Foundation of China (NSFC) under Grants No. U2032103, No. U2032111, No. 11625523, No. 12175239, and No. 12221005, and also by the National Key Research and Development Program of China under Contract No. 2020YFA0406400.

[1] G. S. Adams *et al.* (E852 Collaboration), Observation of pseudoscalar and axial vector resonances in $\pi^- p \to K^+K^-\pi^0 n$ at 18 GeV, Phys. Lett. B **516**, 264 (2001).
[2] M. G. Rath *et al.*, The $K^0_S K^0_S \pi^0$ system produced in $\pi^- p$ interactions at 21.4 GeV/c, Phys. Rev. D **40**, 693 (1989).
[3] F. Nichitiu *et al.* (OBELIX Collaboration), Study of the $K^+K^-\pi^+\pi^-\pi^0$ final state in antiproton annihilation at rest in gaseous hydrogen at NTP with the OBELIX spectrometer, Phys. Lett. B **545**, 261 (2002).
[4] Z. Bai *et al.* (MARKIII Collaboration), Partial-Wave Analysis of $J/\psi \to \gamma K^0_S K^\pm \pi^\mp$, Phys. Rev. Lett. **65**, 2507 (1990).
[5] J.-E. Augustin *et al.* (DM2 Collaboration), Partial-wave analysis of DM2 Collaboration data in the $\eta(1430)$ energy range, Phys. Rev. D **46**, 1951 (1992).
[6] C. Amsler *et al.*, Production and decay of $\eta'(958)$ and $\eta(1440)$ in $p\bar{p}$ annihilation at rest, Eur. Phys. J. C **33**, 23 (2004).
[7] T. Bolton *et al.*, Partial-Wave Analysis of $J/\psi \to \gamma\eta\pi^+\pi^-$, Phys. Rev. Lett. **69**, 1328 (1992).
[8] J.-Z. Bai *et al.* (BES Collaboration), Partial wave analysis of $J/\psi \to \gamma(\eta\pi^+\pi^-)$, Phys. Lett. B **446**, 356 (1999).
[9] J.-E. Augustin *et al.* (DM2 Collaboration), Radiative decay of J/ψ into $\eta(1430)$ and nearby states, Phys. Rev. D **42**, 10 (1990).
[10] M. Ablikim *et al.* (BESIII Collaboration), $\eta\pi^+\pi^-$ Resonant Structure around 1.8 GeV/c^2 and $\eta(1405)$ in $J/\psi \to \omega\eta\pi^+\pi^-$, Phys. Rev. Lett. **107**, 182001 (2011).
[11] M. Acciarri *et al.* (L3 Collaboration), Light resonances in $K^0_S K^\pm \pi^\mp$ and $\eta\pi^+\pi^-$ final states in $\gamma\gamma$ collisions at LEP, Phys. Lett. B **501**, 1 (2001).

[12] J. Z. Bai *et al.* (BES Collaboration), A study of $J/\psi \to \gamma\gamma V(\rho,\phi)$ decays with the BESII detector, Phys. Lett. B **594**, 47 (2004).
[13] D. Coffman *et al.* (MARK-III Collaboration), Study of the doubly radiative decay $J/\psi \to \gamma\gamma\rho^0$, Phys. Rev. D **41**, 1410 (1990).
[14] P. A. Zyla *et al.* (Particle Data Group), The review of particle physics, Prog. Theor. Exp. Phys. **2020**, 083C01 (2020).
[15] T. Barnes, F. E. Close, P. R. Page, and E. S. Swanson, Higher quarkonia, Phys. Rev. D **55**, 4157 (1997).
[16] J. J. Dudek, R. G. Edwards, P. Guo, and C. E. Thomas (Hadron Spectrum Collaboration), Toward the excited isoscalar meson spectrum from lattice QCD, Phys. Rev. D **88**, 094505 (2013).
[17] L. Faddeev, A. J. Niemi, and U. Wiedner, Glueballs, closed fluxtubes, and $\eta(1440)$, Phys. Rev. D **70**, 114033 (2004).
[18] G. S. Bali, K. Schilling, A. Hulsebos, A. C. Irving, C. Michael, and P. W. Stephenson (UKQCD Collaboration), A comprehensive lattice study of SU(3) glueball, Phys. Lett. B **309**, 378 (1993).
[19] C. J. Morningstar and M. J. Peardon, Glueball spectrum from an anisotropic lattice study, Phys. Rev. D **60**, 034509 (1999).
[20] Y. Chen, A. Alexandru, S. J. Dong, T. Draper, I. Horváth, F. X. Lee, K. F. Liu, N. Mathur *et al.*, Glueball spectrum and matrix elements on anisotropic lattices, Phys. Rev. D **73**, 014516 (2006).
[21] C. M. Richards, A. C. Irving, E. B. Gregory, and C. McNeile (UKQCD Collaboration), Glueball mass measurements from improved staggered fermion simulations, Phys. Rev. D **82**, 034501 (2010).
[22] F. Chen, X. Jiang, Y. Chen, K.-F. Liu, W. Sun, and Y.-B. Yang, Glueballs at physical pion mass, arXiv:2111.11929.
[23] J.-J. Wu, X.-H. Liu, Q. Zhao, and B.-S. Zou, Puzzle of Anomalously Large Isospin Violations in $\eta(1405/1475) \to 3\pi$ in the J/ψ Radiative Decay, Phys. Rev. Lett. **108**, 081803 (2012).
[24] X.-G. Wu, J.-J. Wu, Q. Zhao, and B.-S. Zou, Understanding the property of $\eta(1405/1475)$ in the J/ψ radiative decay, Phys. Rev. D **87**, 014023 (2013).
[25] F. Aceti, W. H. Liang, E. Oset, J. J. Wu, and B. S. Zou, Isospin breaking and $f_0(980) - a_0(980)$ mixing in the $\eta(1405) \to \pi^0 f_0(980)$ reaction, Phys. Rev. D **86**, 114007 (2012).
[26] M.-C. Du and Q. Zhao, Internal particle width effects on the triangle singularity mechanism in the study of the $\eta(1405)$ and $\eta(1475)$ puzzle, Phys. Rev. D **100**, 036005 (2019).
[27] M. Ablikim *et al.* (BESIII Collaboration), Study of $\eta(1405)/\eta(1475)$ in $J/\psi \to \gamma K_S^0 K_S^0 \pi^0$ decay, J. High Energy Phys. 03 (2023) 121.
[28] S. X. Nakamura, H. Kamano, T.-S. H. Lee, and T. Sato, Extraction of meson resonances from three-pions photoproduction reactions, Phys. Rev. D **86**, 114012 (2012).
[29] M. Ablikim *et al.* (BESIII Collaboration), First Observation of $\eta(1405)$ Decays into $f_0(980)\pi^0$, Phys. Rev. Lett. **108**, 182001 (2012).
[30] S. X. Nakamura, Q. Huang, J.-J. Wu, H. P. Peng, Y. Zhang, and Y. C. Zhu (to be published).
[31] H. Kamano, S. X. Nakamura, T.-S. H. Lee, and T. Sato, Unitary coupled-channels model for three-mesons decays of heavy mesons, Phys. Rev. D **84**, 114019 (2011).
[32] S. X. Nakamura, Coupled-channel analysis of $D^+ \to K^-\pi^+\pi^+$ decay, Phys. Rev. D **93**, 014005 (2016).
[33] M. Mai, B. Hu, M. Döring, A. Pilloni, and A. Szczepaniak, Three-body unitarity with isobars revisited, Eur. Phys. J. A **53**, 177 (2017).
[34] A. Jackura, C. Fernández-Ramírez, V. Mathieu, M. Mikhasenko, J. Nys, A. Pilloni, K. Saldaña, N. Sherrill, and A. P. Szczepaniak (JPAC Collaboration), Phenomenology of relativistic $3 \to 3$ reaction amplitudes within the isobar approximation, Eur. Phys. J. C **79**, 56 (2019).
[35] M. Mikhasenko, Y. Wunderlich, A. Jackura, V. Mathieu, A. Pilloni, B. Ketzer, and A. P. Szczepaniak, Three-body scattering: Ladders and resonances, J. High Energy Phys. 08 (2019) 080.
[36] M. Bando, T. Kugo, and K. Yamawaki, Nonlinear realization and hidden local symmetries, Phys. Rep. **164**, 217 (1988).
[37] W. H. Press, S. A. Teukolsky, W. T. Vetterling, and B. P. Flannery, *Numerical Recipes 3rd Edition: The Art of Scientific Computing*, 3rd ed. (Cambridge University Press, New York, 2007).
[38] A. Abele *et al.*, $\bar{p}p$ annihilation at rest into $K_L K^{\pm}\pi^{\mp}$, Phys. Rev. D **57**, 3860 (1998).
[39] W. Glöckle, S-matrix pole trajectory in a three-neutron model, Phys. Rev. C **18**, 564 (1978).
[40] B. C. Pearce and I. R. Afnan, Resonance poles in three-body systems, Phys. Rev. C **30**, 2022 (1984).
[41] G. Janssen, K. Holinde, and J. Speth, A meson exchange model for $\pi\rho$ scattering, Phys. Rev. C **49**, 2763 (1994).
[42] M. Mikhasenko, A. Pilloni, M. Albaladejo, C. Fernández-Ramírez, A. Jackura, V. Mathieu, J. Nys, and A. Rodas, B. Ketzer, and A. P. Szczepaniak (JPAC Collaboration), Pole position of the $a_1(1260)$ from τ-decay, Phys. Rev. D **98**, 096021 (2018).
[43] D. Sadasivan, A. Alexandru, H. Akdag, F. Amorim, R. Brett, C. Culver, M. Döring, F. X. Lee, and M. Mai, Pole position of the $a_1(1260)$ resonance in a three-body unitary framework, Phys. Rev. D **105**, 054020 (2022).
[44] N. Suzuki, T. Sato, and T.-S. H. Lee, Extraction of resonances from meson-nucleon reactions, Phys. Rev. C **79**, 025205 (2009).